Superhydrophobic, antiadhesive, and antireflective surfaces mediated by hybrid biomimetic salvinia leaf with moth-eye structures

2014 Appl. Phys. Express 7 087001

(http://iopscience.iop.org/1882-0786/7/8/087001)

Applied Physics Express 7, 087001 (2014)
http://dx.doi.org/10.7567/APEX.7.087001

Superhydrophobic, antiadhesive, and antireflective surfaces mediated by hybrid biomimetic salvinia leaf with moth-eye structures

Cho-Yun Yang[1], Yu-Lin Tsai[2], Cho-Yu Yang[1], Cheng-Kuo Sung[1]*, Peichen Yu[2], and Hao-Chung Kuo[2]

[1]*Department of Power Mechanical Engineering, National Tsing Hua University, Hsinchu 30013, Taiwan, R.O.C.*
[2]*Department of Photonics and Institute of Electro-Optical Engineering, National Chiao Tung University, Hsinchu 30013, Taiwan, R.O.C.*
E-mail: cksung@pme.nthu.edu.tw

Received June 5, 2014; accepted July 1, 2014; published online July 16, 2014

In this paper, we successfully demonstrate multifunctional surfaces based on scaffolding biomimetic structures, namely, hybrid salvinia leaves with moth-eye structures (HSMSs). The novel fabrication process employs scalable polystyrene nanosphere lithography and a lift-off process. Systematic characterizations show the biomimetic HSMS exhibiting superhydrophobic, self-cleaning, antiadhesive, and antireflective properties. Furthermore, the resulting surface tension gradient (known as the Marangoni effect) leads to a superior air retention characteristic in the HSMS under water droplet impact, compared with the traditional hybrid lotus leaf with a moth-eye structure (HLMS). Such results and learnings pave the way towards the attainment and mass deployment of dielectric surfaces with multiple functionalities for versatile biological and optoelectronic applications.

Determining the structures and processes found in nature is the foundation of the field of biomimetics, which has stimulated new ideas for functional surface structures with high adhesion capabilities and for various applications, such as self-cleaning, water harvesting, fluidic drag reduction, and self-healing.[1–4] In recent years, research on biomimetic functional surface structures has focused on controlling the optical properties and wettability of moth-eye and lotus-leaf structures, respectively, in terms of their specific surface capabilities.[5,6] The moth-eye structure consists of a corneal-nipple array, which is a sub-wavelength structure (SWS) that functions as a graded refractive index (GRIN) medium for photons.[7–12] The SWS possesses broadband antireflection characteristics, and the structures can be fabricated using a single-type material (e.g., SiO_2, TiO_2, and ITO) for maintaining optical properties and mechanical durability. In addition, the surface of the moth-eye structure can be superhydrophobic by combining with the lotus-leaf surface.[13–15] The hydrophobic wax crystalloids of the microscale papillae on the surface of lotus leaves were revealed to form an air-retaining layer between a droplet and a structure, thereby producing a superhydrophobic surface.[16–20] Lotus-leaf structures were fabricated by chemical and physical methods, including lithographic, template, and etching methods.[21–24] Contact and sliding angles were generally employed to measure hydrophobic and self-cleaning capabilities. The dynamic effect of the bouncing of a droplet on the lotus-leaf structures was also measured to determine these capabilities under rainy conditions.[25,26]

However, hydrophobic and self-cleaning capabilities may be impaired by liquid impact and wetting of the surface. Therefore, the air retention property of the surface should be enhanced to protect these capabilities. In 2010, Barthlott et al.[27] found that the long-term air retention property of floating *Salvinia molesta* leaves was due to the hierarchical architecture of the leaf surface, which was composed of complex elastic eggbeater-shaped hairs that were coated with nanoscopic hydrophobic wax crystals, except for the tip of the hairs. Yang et al.[28] attempted to biomimic and model a salvinia-leaf structure. In contrast to the lotus-leaf structure, a salvinia leaf exhibits hydrophilic patches on a superhydrophobic surface. Yang et al. proposed the surface tension gradient (the Marangoni effect) of the structure by using theoretical models of wettability to determine the existence of an air-retaining layer. In addition, salvinia-leaf and lotus-leaf structures were fabricated to verify that the air retention property was effectively enhanced in the salvinia-leaf structure.

The purpose of this study was to design a novel biomimetic structure that hybridizes a salvinia leaf with moth-eye structures simultaneously to enhance their air retention properties and maintain antireflection, superhydrophobic, and self-cleaning capabilities. Therefore, a novel process was proposed for fabricating a hybrid salvinia leaf with a moth-eye structure (HSMS) on a thin film. The primary difference between the HSMS and the traditional hybrid lotus leaf with a moth-eye structure (HLMS) was the top surface of hydrophilic patches on the HSMS because of the aforementioned Marangoni effect, which was designed to enhance air retention and create the graded effective refractive index n_{eff}, as shown in Fig. 1(a). In addition, this study not only measured the optical reflectivities of the HSMS and SiN_x single-layer antireflective coating (SL-ARC), but also compared the wettabilities of the HSMS, HLMS, and SL-ARC, which were measured on the basis of contact and sliding angles and the dynamic effect.

A novel process is proposed for fabricating the HSMS and HLMS, which were measured to verify the optical properties and wettability. Figures 1(b)–1(d) illustrate the formation of the HSMS and HLMS, consisting of seven steps. A 500-nm-thick SiN_x layer, which has a refractive index of approximately 1.9 and a nearly zero extinction coefficient, was initially deposited on a 2 in. Si wafer by plasma-enhanced chemical vapor deposition (PECVD). The layer was then treated using oxygen plasma for modifying the hydrophilic surface. The polystyrene (PS) nanosphere technology required numerous adjustments to optimize the single-layer coating, denseness, and uniformity, including the spinning speed and the mixture concentration. In this study, the PS nanospheres of 600 nm diameter, which were mixed in a solution of water and ethanol at 1 : 1 wt %, were uniformly self-assembled on the hydrophilic surface of the SiN_x layer by a two-step spin-coat technique (500 rpm for 10 s and 2000 rpm for 20 s), to act as the sacrificial mask. The structure was removed by inductively coupled plasma reactive ion etching (ICP-RIE) to complete the pattern definition. The bias power and ratio of etching gas flow control the overall etch rate and lateral etching. Therefore, the engineering of the sidewall profile can be achieved by collectively controlling the operating parameters of ICP-RIE.

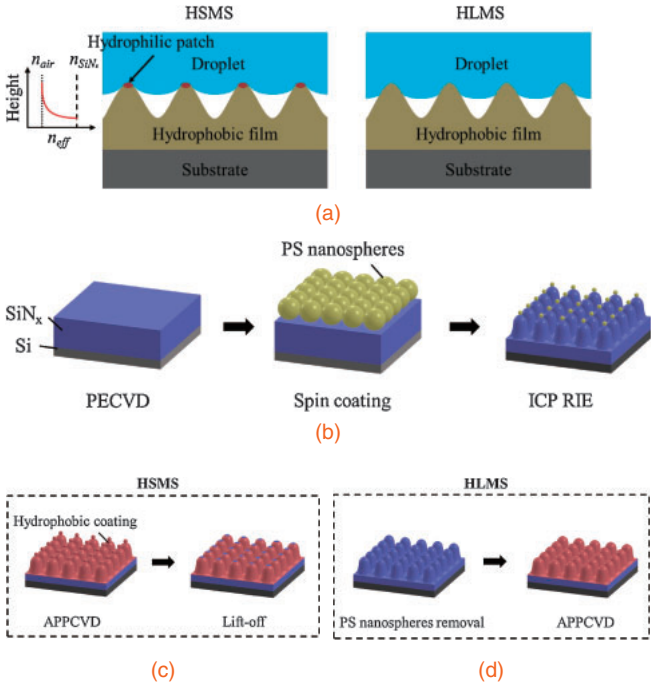

Fig. 1. Schematic of design and fabrication of hybrid biomimetic nanostructures: (a) design, (b) processes of profile definition of structure, (c) HSMS, and (d) HLMS.

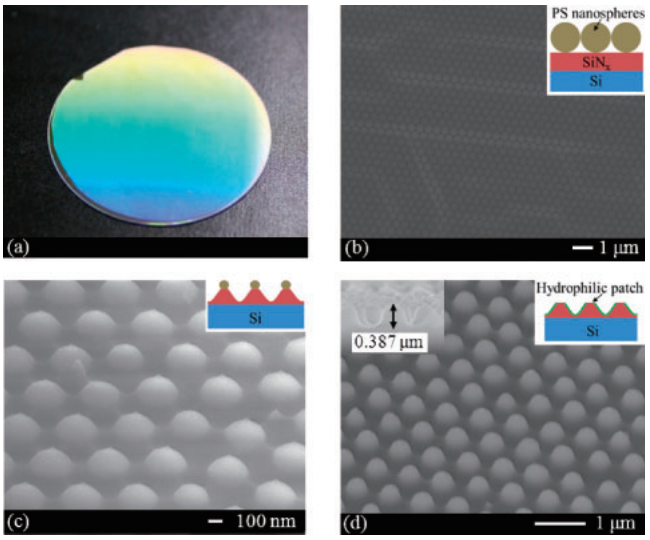

Fig. 2. (a) Photograph of a 2 in. Si wafer with self-assembled PS nanospheres; SEM images of nanostructure (b) coated with PS nanospheres, (c) etched, and (d) treated with the lift-off process.

Table I. Measured results of the static contact, advancing, receding, and sliding angles of HSMS, HLMS, and SL-ARC (in deg).

	HSMS	HLMS	SL-ARC
Contact angle	143.39	156.86	121.51
Advancing angle	149.38	159.22	135.08
Receding angle	136.02	148.84	103.00
Sliding angle	9.72	3.55	51.02

Afterward, two procedures were designed to fabricate the HSMS and HLMS, as shown in Figs. 1(c) and 1(d). In fabricating the HSMS, a thin hydrophobic coating was obtained using the fluoroalkylsilane (FAS) precursor [1*H*,1*H*,2*H*,2*H*-perfluorooctyltriethoxysilane, $CF_3(CF_2)_5CH_2CH_2$-$Si(OCH_2CH_3)_3$], which was applied by atmospheric-pressure plasma chemical vapor deposition (APPCVD).[29] The residual PS nanospheres were removed by a lift-off process to eliminate the hydrophobic properties of the top layer. In the HLMS fabrication, the remaining PS nanospheres were first removed using acetone, and then a thin hydrophobic layer was uniformly applied by APPCVD to ensure a superhydrophobic surface.

Figure 2(a) shows PS nanospheres self-assembled on a 2 in. Si wafer. The uniform gratinglike color dispersion demonstrates the excellent periodicities of the PS nanospheres distributed over the entire substrate. Figure 2(b) shows a scanning electron microscopy (SEM) image of the uniform PS nanosphere monolayer on the Si wafer. The SEM image shows residual PS nanospheres on top of the nipple array after etching [Fig. 2(c)]. The sixfold hexagonal symmetry mimics a moth-eye structure, and the periodic structure was used to enhance the uniformity and antireflective properties. The tilted surface and cross-sectional SEM images of the fabricated HSMS were obtained after the lift-off process, as shown in Fig. 2(d). A small circular area of the SiN_x surface, approximately 100 nm in diameter, was kept for the surface passivation of the residual PS nanospheres, which were covered and then removed in the fabrication process. In addition, a conventional 80-nm-thick SiN_x SL-ARC subjected to hydrophobic treatment by APPCVD was also fabricated on a Si wafer for comparison.

Table I lists the static contact, advancing, receding, and sliding angles that produced various properties of the HSMS, HLMS, and SL-ARC. The measured results indicated that the HSMS and HLMS had superhydrophobic properties at a static contact angle of approximately 150°, and that the SL-ARC was hydrophobic only at a static contact angle of approximately 120°. The sliding angle is generally used to estimate the self-cleaning properties, being the angle at which a water droplet begins to slide on a rough surface. The relationship between the sliding angle and the hysteresis was proposed by Furmidge.[30] The sliding angles of both the HSMS and HLMS were less than 10°, but the angle of the SL-ARC was more than 50°. Therefore, the HSMS and HLMS possess superhydrophobic and self-cleaning properties superior to those of the SL-ARC.

Figure 3 shows the adhesion forces of the HSMS, HLMS, and SL-ARC measured by atomic force microscopy (AFM). The measurement method was proposed by Cappella and Dietler[31] using cantilever loading force-distance curves. In this study, an AFM tip (Nanosensors™ Large Plateau Tips) enabling a 10-μm-diameter surface contact with the structure was used to measure the force-position relationship of large-area surfaces, and the spring constant of the cantilever was 2.8 N/m. The SL-ARC exhibited a higher average adhesive force of 470 nN, and the HSMS and HLMS demonstrated average adhesion forces of 62 and 25 nN with standard deviations of 29 and 14 nN, respectively. The hydrophilic patches of SiN_x were fabricated on top of the HSMS, which led to a larger adhesive force than that of the HLMS. In addition, the adhesive forces of both the HSMS and HLMS were less than 100 nN, which explains why both structures had antiadhesive and stain resistance properties.

Figure 4(a) shows a plot of the optical reflectance spectra of the HSMS, HLMS, and SL-ARC within the wavelength range

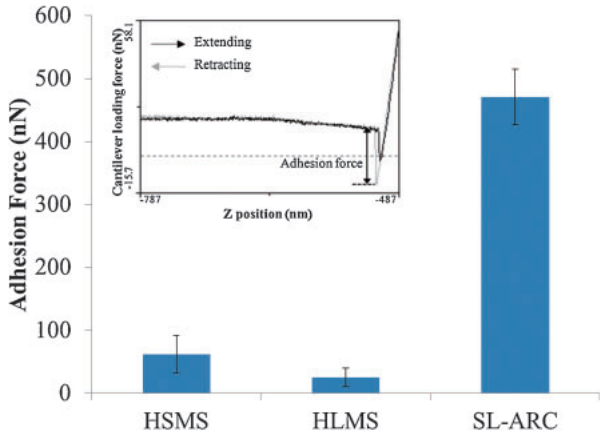

Fig. 3. Adhesion forces of HSMS, HLMS, and SL-ARC, and force-position curves measured by AFM.

of 300–1000 nm. The reflective spectra with respect to different incident angles were measured using a custom-built 15-cm-radius integrating sphere with a motor-controlled rotational sample stage and a spectrometer (Ocean Optics QE65000). A one-sun air mass 1.5, globe (AM1.5G) illumination was used to normalize the reflectance spectra. The lower-level reflection of the SL-ARC within the wavelength range of 500–700 nm may have been caused by destructive interference. Similar reflectance spectra of the HSMS and HLMS were measured and compared with that of the conventional SL-ARC; both structures yielded a relatively broadband antireflective property. Overall, the AM1.5G-spectrum-weighted reflectance of the HSMS and HLMS was approximately 9.5% in the 300–1000 nm wavelength range, which was lower than the 10.4% reflectance of the SL-ARC. In addition, the available SL-ARC rarely achieved a reduction in its higher absolute UV reflectance, which was 35% at a 310 nm wavelength.[11] Figure 4(b) shows the angle-resolved reflectance spectra of the HSMS, HLMS, and SL-ARC within the wavelength range of 400–1000 nm at an incident angle of 0–80°. The reflectance spectra of the SL-ARC increased markedly and produced a relatively rough response when the incident angle increased. In addition, the HSMS and HLMS possessed broadband and omnidirectional antireflective properties. Therefore, both the HSMS and HLMS provide superior AM1.5G-spectrum-weighted reflectance.

Figure 5 shows the contact angles of the HSMS, HLMS, and SL-ARC, which were restored to a steady state by the impact of a 5 μl water droplet at various velocities. A high-speed camera (Photron Fastcam SA3) was used to record the dynamics of the drop impact at a recording rate of 5000 fps. The impact velocity V was defined as an instantaneous velocity at the moment the droplet hits the surface, which was estimated on the basis of the height from which the droplet falls, the volume of the droplet, and the gravitational acceleration. The dynamic pressure of the droplet is determined from the impact velocity as

$$P_{\mathrm{d}} = \frac{1}{2}\rho V^2, \tag{1}$$

where ρ is the density of the droplet. Yang et al.[28] proposed the contact line density method that defined the critical asperity height for assessing the suspension or collapse of the liquid droplet on the salvinia-leaf/lotus-leaf structure.

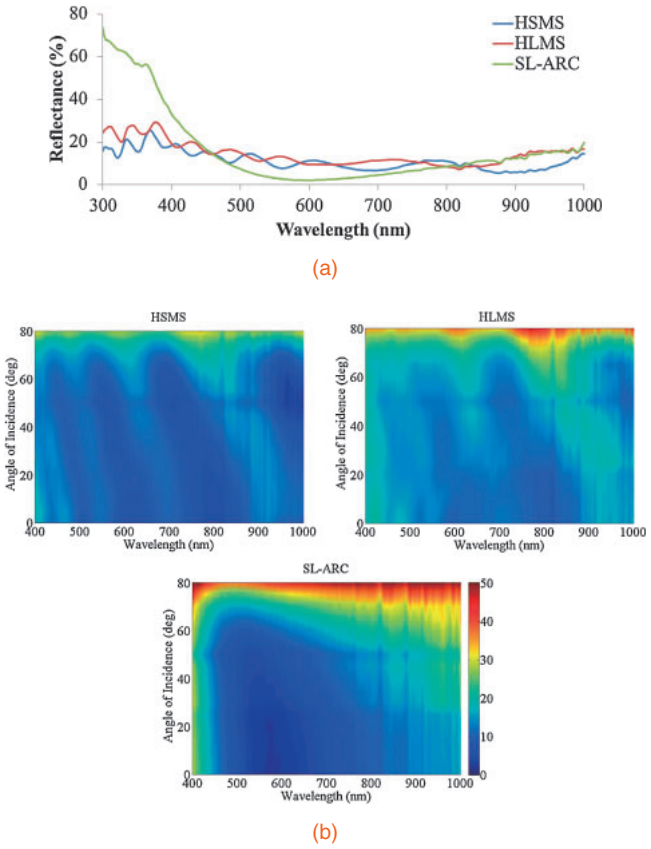

Fig. 4. Measured results of (a) reflectance spectra and (b) angle-resolved reflectance spectra of HSMS, HLMS, and SL-ARC.

The contact line density of the hybrid biomimetic structure is obtained as $\Lambda = \pi d/p^2$, where d is the diameter of the interface between the droplet and the nipple array, and p is the pitch of the nipple array. The unit impact force of the droplet exerted on the structure is

$$F_{\mathrm{i}} = P_{\mathrm{d}} A_{\mathrm{u}}, \tag{2}$$

where A_{u} is the unit projected area of the interface between the droplet and the structure gap, $A_{\mathrm{u}} = 2p^2 - 1/2\pi d^2$.

The contact line density method was determined by balancing impact, surface, and Marangoni forces. The contact line density reaches the critical value

$$\Lambda_{\mathrm{c}} = \frac{-P_{\mathrm{d}} A_{\mathrm{u}}}{2p^2\gamma[\cos(\theta_{\mathrm{a}} + \alpha - 90^\circ) - (\cos\theta_{\mathrm{p}} - \cos\theta_{\mathrm{l}})]}. \tag{3}$$

Here, γ is the surface tension at the liquid vapor, θ_{a} is the advancing angle of the surface material, and α is the included angle between the lateral side and bottom of the nipple. θ_{p} and θ_{l} are the contact angles of the hydrophilic patch and lateral surfaces of the hybrid biomimetic structure, respectively. In the lotus effect, the Marangoni force can be diminished as $\theta_{\mathrm{p}} = \theta_{\mathrm{l}}$. If $\Lambda > \Lambda_{\mathrm{c}}$, the droplet would be suspended on the structure; otherwise, the droplet would penetrate the structure.

Figure 5(a) shows snapshots of the droplet hitting the surface of the HSMS and HLMS at an impact velocity of 0.4427 m/s. The droplet deformed and then retracted and bounced off the surface. The droplet then became steady on the surface with a high contact angle, suggesting the existence of an air layer and a composite interface in a Cassie–Baxter

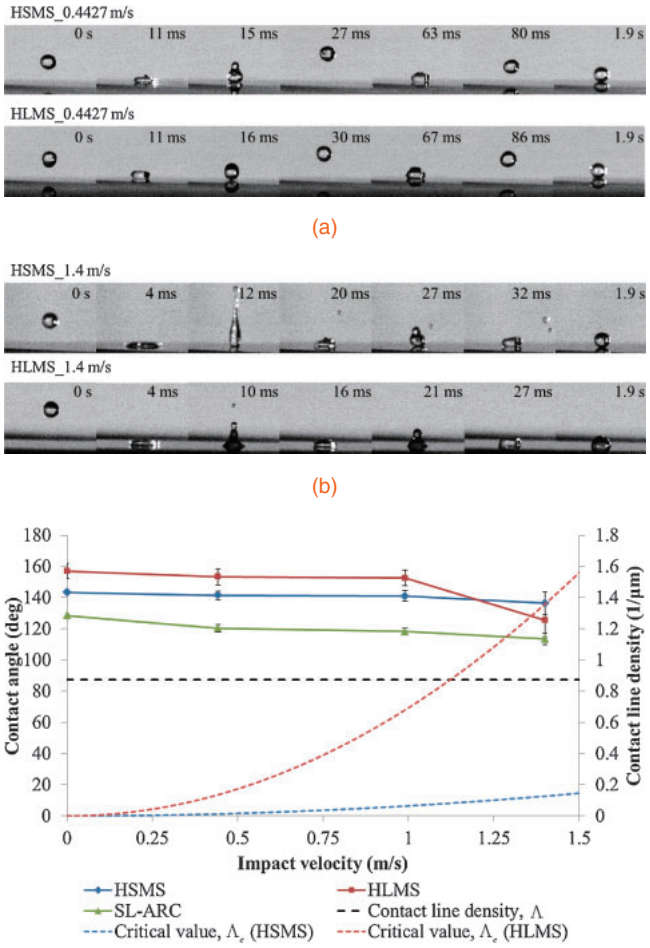

Fig. 5. Snapshots of a 5 μl droplet hitting the surface of HSMS and HLMS at impact velocities of (a) 0.4427 and (b) 1.4 m/s. (c) Steady contact angles and contact line densities obtained after droplet impact at various impact velocities.

state.[19] The droplet did not bounce from the surface of both structures at an impact velocity of 1.4 m/s, and was pinned to the surface during the deformation of the droplet, as shown in Fig. 5(b). A reduced contact angle of the HLMS was created by a homogeneous interface without an air layer after the droplet became steady in a Wenzel state,[18] which was caused by the wetting of the surface. Figure 5(c) shows the relationship between the various impact velocities and steady contact angles of the HSMS, HLMS, and SL-ARC after droplet impact. The steady contact angle of the SL-ARC was consistently reduced as the impact velocity was increased because of the diffusion of the wetting area. As the simulation results, the structure might be wetted when the impact velocity was increased. The steady contact angles of both the HSMS and HLMS after droplet impact at a velocity of 0.4427 m/s were maintained at approximately 150° because of the existence of an air layer. When the impact velocity was increased to 1.4 m/s, the contact angle of the HSMS remained at approximately 140°, but that of the HLMS decreased sharply to less than 125°. On the other hand, the sliding angle of the HSMS remained at 33.4°, but that of the HLMS increased markedly to reach 90°. This phenomenon may be caused by the wetting of the HLMS without an air layer, and the results confirmed that the contact line density was lower than the critical value of the HLMS. By contrast, the Marangoni effect, which is produced by the hydrophilic patches of the HSMS, may have protected and reinstated the air layer. This result confirmed that the air retention and self-cleaning properties were respectively enhanced and maintained after water droplet impact by biomimicking the HSMS.

In this study, we propose the use of a hybrid salvinia leaf with a moth-eye structure (HSMS) for enhancing the air retention and antireflection properties. In contrast to the traditional hybrid lotus leaf with a moth-eye structure (HLMS), a surface tension gradient (the Marangoni effect) is present in this hybrid structure. In addition, a novel process of fabricating both structures was successfully developed on a 2 in. Si wafer by polystyrene nanosphere lithography and a lift-off process. The experimental results indicate that the AM1.5G-spectrum-weighted reflectance was effectively reduced, and the broadband and omnidirectional antireflective properties were obtained using the HSMS, compared with the conventional single-layer antireflective coating (SL-ARC). Moreover, the air retention property of the HSMS was considerably enhanced, and the superhydrophobic and self-cleaning properties were retained even under water droplet impact.

1) B. Bhushan, Philos. Trans. R. Soc. A **367**, 1445 (2009).
2) Y. K. Lai, Z. Chen, and C. J. Lin, J. Nanoeng. Nanomanuf. **1**, 18 (2011).
3) K. K. S. Lau, J. Bico, K. B. K. Teo, M. Chhowalla, G. A. J. Amaratunga, W. I. Milne, G. H. McKinley, and K. K. Gleason, Nano Lett. **3**, 1701 (2003).
4) R. Truesdell, A. Mammoli, P. Vorobieff, F. van Swol, and C. J. Brinker, Phys. Rev. Lett. **97**, 044504 (2006).
5) P. B. Clapham and M. C. Hutley, Nature **244**, 281 (1973).
6) W. Barthlott and C. Neinhuis, Planta **202**, 1 (1997).
7) W. H. Miller, G. D. Bernard, and J. L. Allen, Science **162**, 760 (1968).
8) S. J. Wilson and M. C. Hutley, Opt. Acta **29**, 993 (1982).
9) P. Lalanne and G. M. Morris, Nanotechnology **8**, 53 (1997).
10) J.-Q. Xi, M. F. Schubert, J. K. Kim, E. F. Schubert, M. Chen, S.-Y. Lin, W. Liu, and J. A. Smart, Nat. Photonics **1**, 176 (2007).
11) P. Yu, C. H. Chang, C. H. Chiu, C. S. Yang, J. C. Yu, H. C. Kuo, S. H. Hsu, and Y. C. Chang, Adv. Mater. **21**, 1618 (2009).
12) M. Y. Chiu, C. H. Chang, M. A. Tsai, F. Y. Chang, and P. Yu, Opt. Express **18**, A308 (2010).
13) W. L. Min, B. Jiang, and P. Jiang, Adv. Mater. **20**, 3914 (2008).
14) Y. Li, J. Zhang, S. Zhu, H. Dong, Z. Wang, Z. Sun, J. Guo, and B. Yang, Mater. Chem. **19**, 1806 (2009).
15) Y. Li, J. Zhang, S. Zhu, H. Dong, F. Jia, Z. Wang, Y. Tang, L. Zhang, S. Zhang, and B. Yang, Langmuir **26**, 9842 (2010).
16) C. Neinhuis and W. Barthlott, Ann. Bot. **79**, 667 (1997).
17) T. Young, Philos. Trans. R. Soc. London **95**, 65 (1805).
18) R. N. Wenzel, Ind. Eng. Chem. **28**, 988 (1936).
19) A. B. D. Cassie and S. Baxter, Trans. Faraday Soc. **40**, 546 (1944).
20) A. Marmur, Langmuir **20**, 3517 (2004).
21) D. Öner and T. J. McCarthy, Langmuir **16**, 7777 (2000).
22) A. Pozzato, S. D. Zilio, G. Fois, D. Vendramin, G. Mistura, M. Belotti, Y. Chen, and M. Natali, Microelectron. Eng. **83**, 884 (2006).
23) L. Feng, S. Li, H. Li, J. Zhai, Y. Song, L. Jiang, and D. Zhu, Angew. Chem., Int. Ed. **41**, 1221 (2002).
24) B. Qian and Z. Shen, Langmuir **21**, 9007 (2005).
25) Y. C. Jung and B. Bhushan, Langmuir **24**, 6262 (2008).
26) P. Tsai, S. Pacheco, C. Pirat, L. Lefferts, and D. Lohse, Langmuir **25**, 12293 (2009).
27) W. Barthlott, T. Schimmel, S. Wiersch, K. Koch, M. Brede, M. Barczewski, S. Walheim, A. Weis, A. Kaltenmaier, A. Leder, and H. F. Bohn, Adv. Mater. **22**, 2325 (2010).
28) C. Y. Yang, C. Y. Yang, and C. K. Sung, Jpn. J. Appl. Phys. **52**, 06GF08 (2013).
29) C. L. Wu, C. Y. Yang, T. P. An, J. W. Lin, and C. K. Sung, Appl. Surf. Sci. **261**, 441 (2012).
30) C. G. L. Furmidge, J. Colloid Sci. **17**, 309 (1962).
31) B. Cappella and G. Dietler, Surf. Sci. Rep. **34**, 1 (1999).